CENTENARY OF THE OIV
45th WORLD CONGRESS OF VINE AND WINE
14-18 OCTOBER 2024 FRANCE-DIJON
OIV
Available on IVES Conference Series vine & wine

DOI : https://doi.org/10.58233/LblzEv6k

Non-destructive HIS-based analysis for shelf-life evaluation of table grape

Teodora Basile[1] Carlo Bergamini[1], Maria Francesca Cardone[1], Lucia Rosaria Forleo[1], Luca Nerva[2], Walter Chitarra[2], Antonio Coletta[1], Margherita D'Amico[1], Antonio Marsico[1] and Rocco Perniola[1]

[1] Consiglio per la Ricerca in agricoltura e l'analisi dell'Economia Agraria-Centro di Ricerca Viticoltura ed Enologia (CREA- VE), via Casamassima, 148, 148-70010 Turi (BA), Italy.
[2] Consiglio per la Ricerca in agricoltura e l'analisi dell'Economia Agraria-Centro di Ricerca Viticoltura ed Enologia (CREA- VE), Via XXVIII Aprile 26, 31015 Conegliano (TV), Italy

Abstract. A visible change in the appearance of a fresh product often negatively impacts the perceived quality from a consumer's point of view. This is particularly evident in fresh table grapes, for which rachis browning results in a sudden drop in its selling price. Early detection of browning could help implement preventive strategies, leading to economic savings. To monitor rachis browning onset on a novel table grape variety during cold storage, a Hyperspectral Specim IQ camera was used to record 3D images in the Vis-NIR range (400-1000 nm). After image acquisition, the Specim IQ Studio software was used for the classification of regions of interest (ROIs), which were used to build false color masks for the amount of browning of rachides.

1. Introduction

For fresh table grapes, rachis browning is one of the main external modifications that affect their quality during storage and decreases grape value [1]. Usually, rachis browning is evaluated by subjective color scale based image analysis methods in the visible range. However, this subjective evaluation of rachis browning is prone to errors and can be influenced by various factors such as the compactness of the cluster, the color of the berries, and the level of decay. Additionally, the evaluator's proficiency, level of training, and workload also play an important role. This is because the analyst has to simultaneously take into account the browning intensity, the decrease in green color intensity, and the reduction in rachis thickness due to water loss [2]. Moreover, these methods evaluate the browning only after its visible onset, which means that it has already impacted the perceived quality and decreased the product's value. Our investigation was based on two known facts: rachis browning is linked to water and chlorophyll loss, and it involves a modification of the internal cellular structure [3, 4]. The green chlorophyll pigment can be detected in the visible portion of the electromagnetic spectrum, while the water molecules show strong absorption in the NIR (near-infrared) region. Moreover, the NIR region can also be used to investigate modifications in the cellular structures. Therefore, we followed the onset of browning in the visible-NIR range. Hyperspectral Imaging (HSI) is a rapid, accurate, and non-destructive analytical method for assessing food quality. Hyperspectral images generally consist of hundreds of bands (each bands contains a precise number of wavelength) collected in the ultraviolet or visible to the infrared range [5]. This technique provides both spatial and spectral information since each image is a hyperspectral 3D data cube containing a sequence of consecutive sub-images taken at various wavelength bands covering the whole surface of the object [6]. By extracting each pixel in this 3D object, it is possible to visualize the spectral fingerprint of that point, which is uniquely linked to its specific chemical composition [7]. The possibility of having specific, point-by-point information of the whole specimen under investigation enables the selection of areas of interest in which a change is taking place (e.g., browning) and allows tracking changes simply by collecting sequential HIS images.

2. Material and methods

2.1. Grape samples

The table grape variety employed in this study, named Aika [8], was obtained as part of an ongoing breeding program carried out in our research center CREA-VE of Turi (BA) Southern Italy and was harvested from vineyards growing in the same area. After harvest, the bunches were immediately analyzed (T1) and then packed

in cardboard boxes and stored at 2°C with 95% relative humidity. The samples were stored in the absence of sulfur dioxide (SO_2), which is the most important preservative used during the commercial storage and shipping of table grapes. We chose not to use SO_2 generating pads since this compound can alter the color of the rachis from yellowish to khaki modifying the natural transition from green to brown of the rachis [2]. Therefore, it would have added a source of uncontrolled color variability.

Before each measurement, the bunches were left to cool down to the set room temperature (25°C). The measurements were performed over 14 days, every 3 to 4 days until the onset of browning for a total of 5 time points collected including the harvest (T1 to T5). To follow the onset of browning on rachis we did not remove the berries since it would have made it impossible to repeat the measurement on the same intact bunch. This means that due to the presence of berries, it was difficult to observe the internal part of the rachis. The changes were followed on the visible portion of the rachides, which is the main part visible to consumers.

2.2. Image acquisition and processing

A Specim IQ camera was employed to acquire 3D images in the Vis-NIR range (400-1000 nm). In the laboratory each grape bunch was placed against a black background and fully illuminated by halogen tungsten lamps, the setup is displayed in Figure 1. The spatial resolution of the recorded data is 512x512 pixels, the number of total bands is 204, and the spectral resolution (FWHM) is 7 nm.

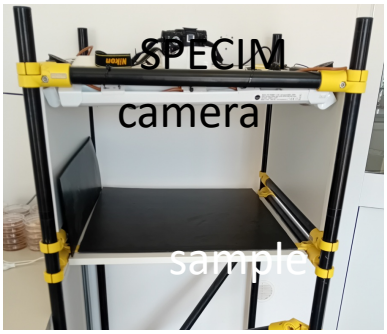

Figure 1. Image collection setup in the laboratory.

Prior to the analysis, a black-and-white correction was performed on the spectral images. A dark image and a white image were obtained respectively by covering the lens with a cap and collecting an image of a standard white reference [9]. The corrected image (R_s) was calculated according to the following equation:

$$R_s\,(l,t) = (R_0 - R_d)/\,(R_t - R_d) \qquad (1)$$

where R_0 is the original hyperspectral image, R_d is the dark image and R_t is the white reflectance image [10]. To remove redundant wavebands and decrease the high dimensionality of the data we performed a PCA.

We applied two algorithms for image classification: unsupervised K-means clustering with Python 3.12.3 and supervised SAM (Spectral Angle Mapper) with the Specim IQ Studio software.

From selected ROIs (regions of interest) the mean spectral profiles were preprocessed with a Savitzky Golay smoothing (filter width 15 and polynomial order 2).

3. Results

A classification procedure**,** given a set of observations (i.e., the pixel represented as vectors in a hyperspectral image), tries to allocate a unique label to each pixel vector [11]. The unsupervised K-means clustering did not allow a classification based on the different browning levels. It seems that the classification outcome was affected by the non-homogeneous illumination of the sample. Even focusing only on the rachis, its tridimensional shape results in shadowing of the side curved regions. This is probably due to the reflection following a Lambertian response [12] with obliquely oriented pixels near the edges contributing a weaker intensity of radiation reflected back to the camera.

Therefore, we decided to perform a supervised image classification which can be either based on pixel information or based on the use of training samples. In our case, such as in natural environments, it is difficult to find labeled training samples [13]. This is especially true if you want to predict future browning based on “pre-browning“ classes.

In the onset of rachis browning, the visible appearance of brown spots is the final step. Between the “healthy and visibly green” and “damaged and visibly brown” steps the rachis cells and their molecular composition undergo a gradual change. This change, although not easy to follow by the naked human eye, is evident in the modification of the spectral profile (Figure 2). Therefore, based on the rachis portion that turned brown at the final time point collected (T5), we selected the same regions at the previous time points (T1 to T4). Those areas even still greenish looking in the future days were going to become brown, thus representing “pre-brown” pixels.

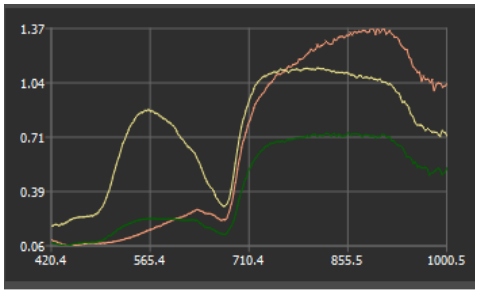

Figure 2. Example of spectral profile (% reflectance vs nm) of target classes: healthy (in yellow), pre-brown (in green) and visibly brown (in orange).

The selection of ROIs area is of pivotal importance. We wanted to select rachis areas large enough to extract an effective reference mean spectra for the pre-brown class at each time point. As observed with the reflection issues encountered with the unsupervised classification linked to the shape of the rachis, we needed to select a small area

(few pixels) of the whole rachis. In a recent study, researchers evaluated the effect of the ROIs size on the classification of wheat seeds. They found that even if more pixels can improve the signal-to-noise ratio through pixel averaging, the curved surface of the seeds causes non-uniform diffuse reflection, which has a strong detrimental impact. A flatter but smaller ROI area, despite the higher level of random noise associated with the ROI mean area, was found to be more effective for the classification, since it is least prone to non-uniformities in diffusely reflected light [14].

The SAM algorithm employed determines the spectral similarity (smaller spectral angle) between an image spectrum and a reference spectrum (e.g. from a ROI) of each pixel in the hyperspectral data. Choosing smaller and carefully selected the ROIs as input for the supervised SAM classification allowed us to correctly classify areas of the rachis as "pre-brown" in contrast to those still healthy and already brown (Figure 3).

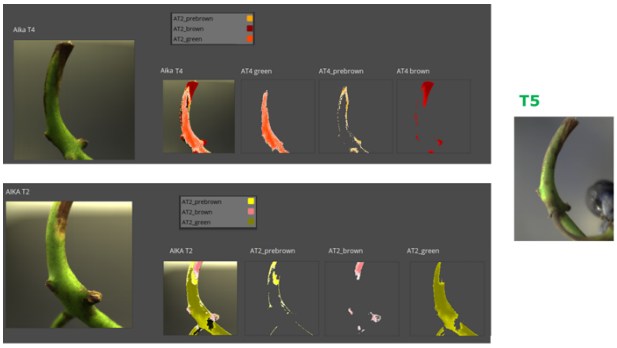

Figure 3. SAM classification of two time points T2 and T4 based on browning at T5 for Aika variety. The darker the spectral pixels in the image the higher the similarity to the reference spectrum.

It was not possible to classify any pixel at harvest (T1) other than belonging to "healthy green" (Figure 4). That is expected since the bunches analyzed at T1 were brought to the lab immediately after harvest, thus the whole rachis is still green and healthy.

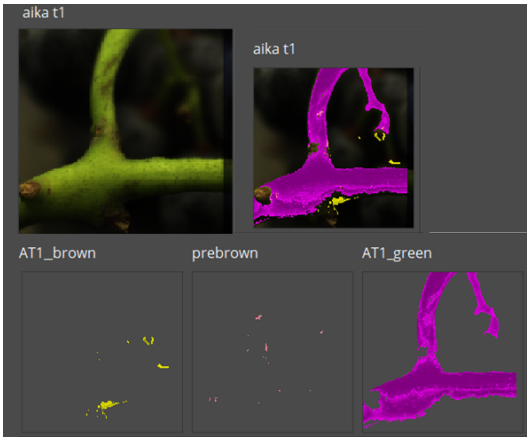

Figure 4. SAM classification of T1 (harvest) based on browning at T5 for Aika variety.

Moreover, we found that the classification models are variety-dependent; they are not able to classify other varieties (Figure 5).

Figure 5. SAM classification of T3 based on browning at T5 for the novel Vigilarum variety using pre-brown class created for Aika variety.

The SAM analysis determines reasonable classification with a good concordance to the visual perception, as shown in the figures. We found that the accuracy of the prediction is in accordance with the future browning with sometimes overlaps in the classification. Unfortunately, a quantitative evaluation of the SAM result was not supported by the used version of Specim IQ Studio. The main advantage of the software is that once these classes are created it is possible to display rachis classification upon taking a picture (Figure 6).

Figure 6. Example of SAM classification on the camera display.

4. Conclusion

Maintaining the quality of fresh fruits often is a matter of visual appearance. Our studies aim to find a spectral region that can track the changes in the rachides before browning onset to allow the adoption of proper selling strategies. Carefully selecting ROIs areas, three classes have been created with a supervised SAM algorithm: healthy, brown, and pre-brown. The classification was performed on the camera's own software (Specim IQ Studio). To comply with FAIR principles [15], we are currently implementing supervised classification algorithms in Python using the selected ROIs as inputs. These algorithms could be used with images collected with any HIS camera.

5. References

1. N. Hamie, J.P. Zoffoli, L. Tarricone, V. Verrastro, A.G. Pérez-Donoso, G. Gambacorta, Postharvest Biol. Technol 184, 111758 (2022), https://doi.org/10.1016/j.postharvbio.2021.111758.

2. A. Bahar, T. Kaplunov, V. Alchanatis, A. Lichter, Postharvest Biol Technol 134, 106-113 (2017), https://doi.org/10.1016/j.postharvbio.2017.08.016.

3. M. Blanco, I. Villarroya, TrAC Trends Anal. Chem., 21(4), 240-250 (2002), https://doi.org/10.1016/S0165-9936(02)00404-1.
4. M. R. Slaton, E. R. Hunt, W. K. Smith, Am. J. Botany, 88(2), 278–284 (2001), https://doi.org/10.2307/2657019
5. M.J. Khan, H.S. Khan, A. Yousaf, K. Khurshid, A. Abbas, IEEE 6, 14118–14129 (2018).
6. M.E. Paoletti, J.M. Haut, J. Plaza, A. Plaza, ISPRS J. Photogramm. Remote Sens. 158, 279–317 (2019),
7. T. Basile, D. Mallardi, M.F. Cardone, Chemosensors (2023), 11, 579. https://doi.org/10.3390/chemosensors11120579
8. Novel grapes from ValNuVaut project https://www.valnuvaut.it/wp-content/uploads/2022/09/AIKA-N.pdf
9. J. Qiao, M.O. Ngadi, N. Wang, C. Gariépy, S.O. Prasher, J. Food Engineering, 83(1), 10-16 (2007), https://doi.org/10.1016/j.jfoodeng.2007.02.038
10. Y. Sun, X. Gu, K. Sun, H. Hu, M. Xu, Z. Wang, K. Tu, L. Pan, LWT, 75, 557-564 (2017), https://doi.org/10.1016/j.lwt.2016.10.006.
11. P. Ghamisi, J. Plaza, Y. Chen, J. Li, A. J. Plaza, IEEE Geoscience and Remote Sensing Magazine, 5(1), 8-32 (2017), doi: 10.1109/MGRS.2016.2616418.
12. G.F.A. Kortüm, Reflectance spectroscopy: principles, methods, applications translated from the German by James E. Lohr. (Berlin: Springer ; 1969)
13. Z. Han, J. Gao, Comput. Electron. Agr. 164, 104888 (2019), https://doi.org/10.1016/j.compag.2019.104888.
14. S.R. Delwiche, I. Baek, M.S. Kim, Biosyst. Eng., 212, 106-114 (2021), https://doi.org/10.1016/j.biosystemseng.2021.10.003.
15. M. Wilkinson, M. Dumontier, I. Aalbersberg, et al., Sci Data 3, 160018 (2016), https://doi.org/10.1038/sdata.2016.18